Journal of Materials Chemistry A

ROYAL SOCIETY OF CHEMISTRY

REVIEW

View Article Online
View Journal | View Issue

Cite this: J. Mater. Chem. A, 2021, 9, 18148

The crucial roles of the configurations and electronic properties of organic hole-transporting molecules to the photovoltaic performance of perovskite solar cells

Weidong Ling,[a] Fan Liu,[a] Qianqian Li *[a] and Zhen Li *[ab]

Received 3rd May 2021
Accepted 3rd August 2021

DOI: 10.1039/d1ta03718h

rsc.li/materials-a

Perovskite solar cells have become one of the most promising technologies to make use of solar energy; to date, the power conversion efficiencies (PCEs) have been improved from 3.8% to 25.6%. Hole-transporting materials (HTMs) play an important role in the photovoltaic conversion process by extracting photogenerated holes and transporting charges. However, the relationship among the molecular structure of HTMs, molecular packing in hole-transporting layers (HTLs) and the device performance of perovskite solar cells (PSCs) has not been explained systematically. In this review, the structure–property relationship of HTMs is discussed from the aspects of molecular configuration, electron properties, and their synergetic effects, to provide useful guidance for the HTM design and PSC development.

1. Introduction

There is no doubt that solar energy is the most important and abundant kind of renewable energy source, and the development of solar cells with high-efficiency, low-cost and long-term stability has attracted extensive attention from both academia and industry.[1–3] Among them, perovskite solar cells (PSCs) have been considered as one of the most promising photovoltaic (PV) technologies toward commercialization,[4–10] for their rapidly increased power conversion efficiencies (PCEs, from 3.8% (ref. 11) in 2009 to 25.6% (ref. 12) at present).

PSCs consist of a transparent conducting oxide (TCO), electron transport layer (ETL), perovskite layer, hole transport layer (HTL) and metal electrode. According to their related positions, PSCs can be classified as conventional n–i–p devices (Fig. 1a) and inverted p–i–n devices (Fig. 1b), both of which have a similar mechanism as briefly shown in Fig. 1c. It is essential that photogenerated electrons and holes are created in perovskite layer, and then HTL together with ETL, extract and transport the charge carriers to the cathode or anode (processes 1, 2, and 3); however, many possibilities of charge recombination (process 4–7) are unavoidable and need to be controlled.

In the PV processes of PSCs, hole-transporting materials (HTMs) as the middle layer can extract photogenerated holes

[a]Hubei Key Lab on Organic and Polymeric Opto-Electronic Materials, Sauvage Center for Molecular Sciences, Department of Chemistry, Wuhan University, Wuhan 430072, China. E-mail: qianqian-alinda@163.com; lizhen@whu.edu.cn
[b]Institute of Molecular Aggregation Science, Tianjin University, Tianjin 300072, China

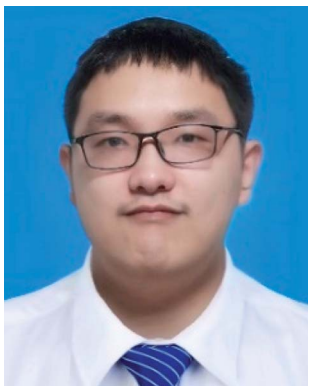

Weidong Ling received his Bachelor's degree from the College of Chemistry and Molecular Science at Wuhan University in 2020. He is currently a Master's graduate student under the supervision of Prof. Zhen Li. His research mainly focuses on the design and synthesis of organic hole-transport materials for perovskite solar cells.

Fan Liu obtained his Bachelor's degree from Huanggang Normal University in 2014, and then obtained his PhD degree under the supervision of Prof. Zhen Li and Prof. Qianqian Li at Wuhan University in 2020. His research mainly focuses on the design and synthesis of hole-transporting materials for perovskite solar cells.

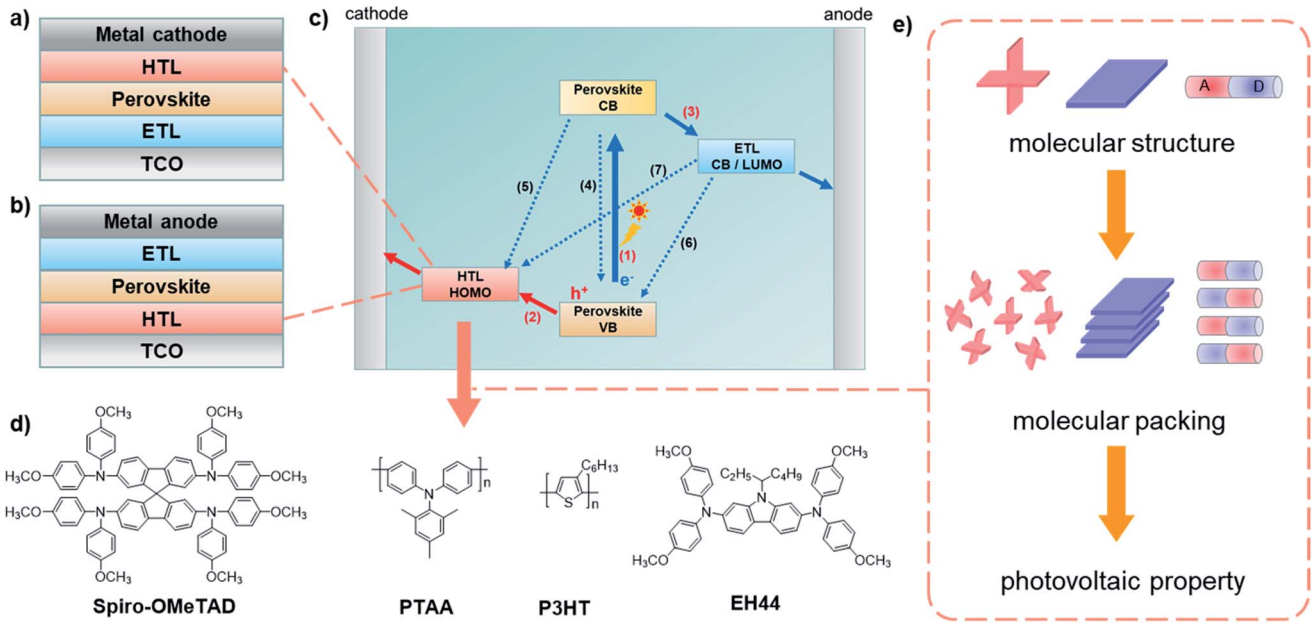

Fig. 1 (a) Device architecture of conventional n–i–p perovskite solar cells. (b) Device architecture of inverted p–i–n perovskite solar cells. (c) Schematic representation of the mechanism and electron transfer processes in perovskite solar cells. (d) Chemical structures of several representative HTMs. (e) The relationship among molecular structure, molecular packing and photovoltaic properties of HTMs.

from the perovskite and transport charges to the back contact metal electrode (in conventional n–i–p devices) or front glass electrode (in inverted p–i–n devices); they also block the electron transfer to the electrode and decrease the defects of the perovskite layer in some cases, to effectively reduce the possible charge recombination at the interface, contributing to the improved photovoltaic performance.[13–23] The commonly used HTMs can be simply divided into inorganic materials, such as NiO_x,[25] CuSCN,[26] CuI,[27] *etc.*, and organic materials, such as **spiro-OMeTAD**,[28] PTAA,[29] P3HT,[30] and EH44 [31] (Fig. 1d). Among them, organic small-molecule HTMs have drawn much attention due to their easy synthesis, the convenience of modification, low cost, and good reproducibility.[13–15,32–35] However, they still exhibit the drawback of low conductivity and hole-mobility with poor film morphology. Thus, some dopants, such as bis(trifluoromethanesulfonyl)imide (Li-TFSI), 4-*tert*-butylpyridine (*t*-BP) and tris[2-(1*H*-pyrazol-1-yl)-4-*tert*-butylpyridine] cobalt(III)-tris[bis(trifluoromethylsulfonyl)imide] (FK209), have been added in many cases, which has proved to be an efficient approach to improve conductivity. Due to the migration of ions, the hydrophilicity of metal-salts and the incompatibility among the different components, the stability of doped PSCs usually decreases with the extra pinholes in HTLs and unfavorable reactions with polar molecules such as H_2O and O_2. In contrast, dopant-free HTMs can contribute to the stability of PSCs, while their photovoltaic performance is not always as good as doped ones for the weakness of hole mobility and conductivity, which are mainly related to the aggregated state of hole-transporting molecules.[15,36–40]

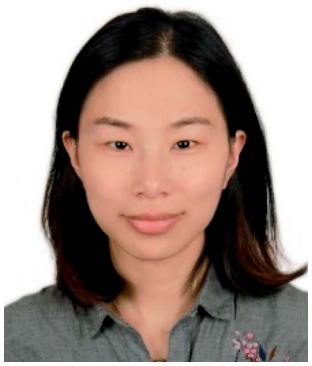

Qianqian Li received her B.Sc. degree from Hubei University, China, in 2004, and then obtained her PhD degree under the supervision of Prof. Zhen Li at Wuhan University in 2009. She is now a full professor at Wuhan University, and her research interests include the design and synthesis of new optoelectronic functional materials.

Zhen Li received his B.Sc. and PhD degrees from Wuhan University (WHU) in China in 1997 and 2002, respectively, under the supervision of Prof. Jingui Qin. He has been a full professor at WHU since 2006 and chair professor at Tianjin University since 2018. His research interests include the development of organic molecules and polymers with new structures and new functions for organic electronics and photonics.

To improve the photovoltaic performance and stability of PSCs, many efficient organic small-molecule HTMs have been explored by the adjustment of their aggregated behaviors in the thin films, which can optimize the film morphology and crystallinity, resulting in increased hole mobility and conductivity.[41–43] Although a large number of studies have focused on molecular aggregates, and many efficient strategies have been proposed, the relationship among the molecular structure, aggregated behavior (molecular packing), and photovoltaic performance of PSCs (Fig. 1e) has not been explained systematically. This may be related to the complex carrier transfer processes and ambiguous molecular packing in the HTLs. Fortunately, in other optoelectronic fields, for instance, organic room-temperature phosphorescence, second-order non-linear optics, mechanoluminescence materials and organic solar cells, it has been scientifically discussed how molecular structures determine various packing modes in aggregate states and further affect optical properties.[45–48] Molecular configurations and electron properties have been proved to be the essential factors, which make it feasible to explain and predict the photovoltaic performance of HTMs from these aspects. Thus, this review provides insight into the structure–property relationship of HTMs by the rational analysis from the single-molecule to aggregated states in PSCs, providing useful guidance to further promote the development of PSCs by efficient molecular design.

2. Hole-transporting materials

An efficient HTM is one of the premises of efficient PSC devices for the function of hole extraction and transport.[49] Accordingly, the essential requirement of HTMs is the suitable energy levels of the highest occupied molecular orbital (HOMO) and lowest unoccupied molecular orbital (LUMO) energy levels to match those of the perovskite layer. Also, efficient HTMs require the following features:

(a) High hole mobility and conductivity, which can decrease the series resistance in the photovoltaic processes, resulting in the increased current. In general, the hole mobility of HTM can be measured by space-charge-limited current (SCLC), time of flight (TOF), field-effect transistor (FET), and transient electroluminescence (TEL) methods. For HTMs in PSCs, SCLC is the most common method, mainly due to the low requirements for the equipment and thickness of materials, and the film state is similar to that of HTMs in PSC devices.[24]

(b) Good solubility and film-forming properties, which are beneficial to the processes of spin-coating fabrication, favoring the optimization of molecular packing, film morphology and the interface contact with perovskite or TCO layer. Better solubility enables a wider concentration range of HTM precursors and more selectable solvents, making it possible to choose the most suitable spin-coating conditions for each HTM, which impact the molecular packing, thickness and morphology of HTLs, resulting in optimal optoelectronic performance.

(c) Stability, including thermal, photochemical and moisture stability. This is essential to the operational lifetime and commercialization of PSCs.

(d) Interfacial interactions. Interface modification or defect passivation can increase the fill factor (FF) by suppressing the charge recombination, contributing to the high conversion efficiencies. Anchoring and Lewis-based groups have been applied in HTMs to improve the interfacial interactions.[43,44,58]

The low price of raw materials, easy synthesis and good reproducibility of HTMs are equally important for large-scale application and commercialization of PSCs. All of these are strongly related to the molecular design of HTMs and their varied aggregated states in the thin films, as determined by the molecular configuration and electronic properties of organic HTMs.

2.1 The main effect of molecular configuration on photovoltaic performance

Molecular configuration is the permanent geometry that derives from the spatial arrangement of covalent bonds and atoms, just like the fixed three-dimensional relationship of the atoms in a molecule, as defined by the bonds between them. For the hole-transporting molecules with conjugated systems as rigid structures, various configurations are mainly determined by the core structures and the linkage modes of different peripheral moieties.[50] These can affect molecular packing *via* steric hindrance, mainly contributing to the varied hole mobilities and conductivities in aggregated states.[53,67]

2.1.1 Planarity of core groups. As a popular organic HTM in PSC devices, **spiro-OMeTAD** has become the most common benchmark with the highest conversion efficiency of 25.17%.[51] It exhibits good solubility and film-forming properties, however low conductivity and hole mobility are unavoidable. This is mainly related to the orthometric structure of 9,9′-spirobifluorene (SBF) as the core unit, resulting in the twisted molecular configuration of the **spiro-OMeTAD** with SBF core, and the molecular parallel π–π stacking with the vertical distance of about 3.8 Å (slightly longer than a distance characteristic of closely packed π–π systems), which can be proved by the single-crystal structure.[52] Thus, the planarity of hole-transporting molecules is essential to improve the hole-transporting property, which is strongly related to the core unit with various shapes. As shown in Fig. 2, a series of core units with different geometries were exploited to adjust the molecular configurations of HTMs, and some relationships between the core structures and photovoltaic performance are summarized.

The molecular configuration of core units is the key factor in the photovoltaic performance of HTMs. For instance, as shown in Fig. 3, once the tetra-thienylethene (TTE) core with the much twisted structure was partially locked by the fused ring, the resultant compound **TTE-2** exhibited lower series resistance and higher FF as the hole transporting layer (HTL), as compared to those of **TTE-1** with the original TTE core. Accordingly, the hole mobility increased from 8.70×10^{-5} to 6.18×10^{-4} cm^2 V^{-1} s^{-1}, and the PCE of the dopant-free PSC device was enhanced from 13.68% to 20.04%.[53]

HTMs with twisted cores usually exhibit good solubility and film-forming properties; however, the branched structures with possible steric hindrance can result in loose molecular packing

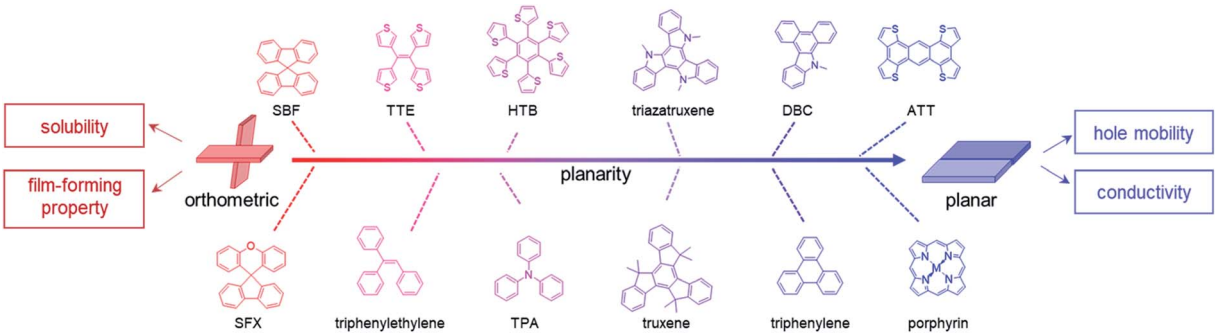

Fig. 2 Various core units of HTMs with different shapes.

molecular configuration (R = 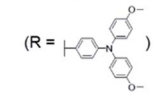)	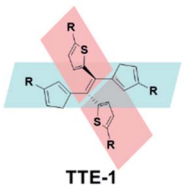 TTE-1	 TTE-2
series resistance R_s / Ω·cm²	5.31	3.52
hole mobility μ_h / cm² V⁻¹ s⁻¹	8.70 × 10⁻⁵	6.18 × 10⁻⁴
fill factor (*FF*)	0.717	0.775
PCE	13.68%	20.04%

Fig. 3 Molecular configurations and device performance of TTE-1 and TTE-2.

in most cases, leading to low conductivity and hole mobility. Thus, the addition of dopants is essential for optimizing the hole transporting properties of these HTMs.[39,81–83] On the other hand, HTMs with planar cores favor π–π interactions in the aggregated states, resulting in compact molecular packing in many cases.[54,55,84–88] This is beneficial for increasing the hole mobility in principle, which can form efficient dopant-free HTLs.[38,39] However, these are usually accompanied by poor solubility and bad film morphology for their good crystallinity.[53,56] Thus, the rational design of core units from twisted structures (Fig. 4 and Table 1) to planar ones (Fig. 5 and Table 2) with tunable configurations, has been proved as an efficient strategy for adjusting the photovoltaic performance of HTMs in different kinds of PSCs.

Compared to the common SBF core in **spiro-OMeTAD**, an orthometric spiro-[fluorene-9,9′-xanthene] (SFX) moiety with the additional oxygen atom in the conjugated bridge can slightly reduce the planarity and the symmetry as the core unit, leading to the slightly lower conductivity of the resultant compound **X60** (1.1×10^{-4} S cm^{-1}) than that of **spiro-OMeTAD** (1.5×10^{-4} S cm^{-1}), and higher hole mobility of 1.9×10^{-4} cm^2 V^{-1} s^{-1}, as compared to **spiro-OMeTAD** (8.1×10^{-5} cm^2 V^{-1} s^{-1}). A 19.84% PCE of doped **X60** devices was achieved, which was close to the PCE record of **spiro-OMeTAD** at that time (20.8% in 2016), meanwhile, the cost of the SFX core (1.12 $ per g) in **X60** is only 3.3% of the SBF core (33.89 $ per g) in **spiro-OMeTAD**.[57] Replacing phenyl in the SBF core with thienyl, the spiro-cyclopenta[2,1-*b*:3,4-*b*′]dithiophene (s-CPD) core was designed by Marius and coworkers. The hole mobility of **s-CPDTOMe** films increased to 3.0×10^{-5} cm^2 V^{-1} s^{-1} after light soaking treatments, and **s-CPDTOMe** without dopants performed well in PSC devices and obtained a PCE of 13.4% and an FF of 0.72, mainly due to the defect passivation effect of sulfur atoms and appropriate treatment for HTM films.[58]

Apart from the orthometric feature by spiro structures as the core moieties, the slightly twisted configuration of HTMs can also be constructed by large peripheral moieties linked to the cores with small sizes. For instance, triphenylethylene with three phenyl moieties linked to the ethenyl unit exhibited dihedral angles of 30.91°, 60.19°, and 28.21° between these moieties, respectively. The twisted and asymmetric core leads to good solubility and film-forming properties of **CJ-01**;[59] the resultant HTL showed a slightly less rough morphology with smaller pinholes than that of the **spiro-OMeTAD** film. Accordingly, the **CJ-01**-based PSC exhibited a PCE of 18.56% with an FF of 0.747, which are close to those of **spiro-OMeTAD** based devices (PCE: 18.69%, FF: 0.760) under the same conditions. The stability of the unsealed **CJ-01**-based device is also slightly better; 67.0% of original PCE can be retained after 85 °C thermal storage for 120 h, and 69.2% after AM 1.5 G illumination (100 mW cm^{-2}) for 90 h, as compared with 63.3% and 65.9% for **spiro-OMeTAD** based devices under the same conditions, respectively. Similarly, phenyl-substituted thieno[2,3-*b*]thiophene, with dihedral angles of 43.3°, 62.4°, 55.7°, and 46.1° between each phenyl moiety and the thieno[2,3-*b*]thiophene plane by calculation, was employed in compound **XY1** as the twisted core.[60] It exhibited a smooth morphology with a low roughness RMS of 0.4 nm, and a high hole mobility of 3.76×10^{-4} cm^2 V^{-1} s^{-1} was achieved. This is beneficial to the fabrication of dopant-free devices, and a PCE of 18.78% was achieved in inverted PSCs. For the hexakis(2-thienyl)benzene (HTB) core with a propeller-shape, the helical symmetry structure can be

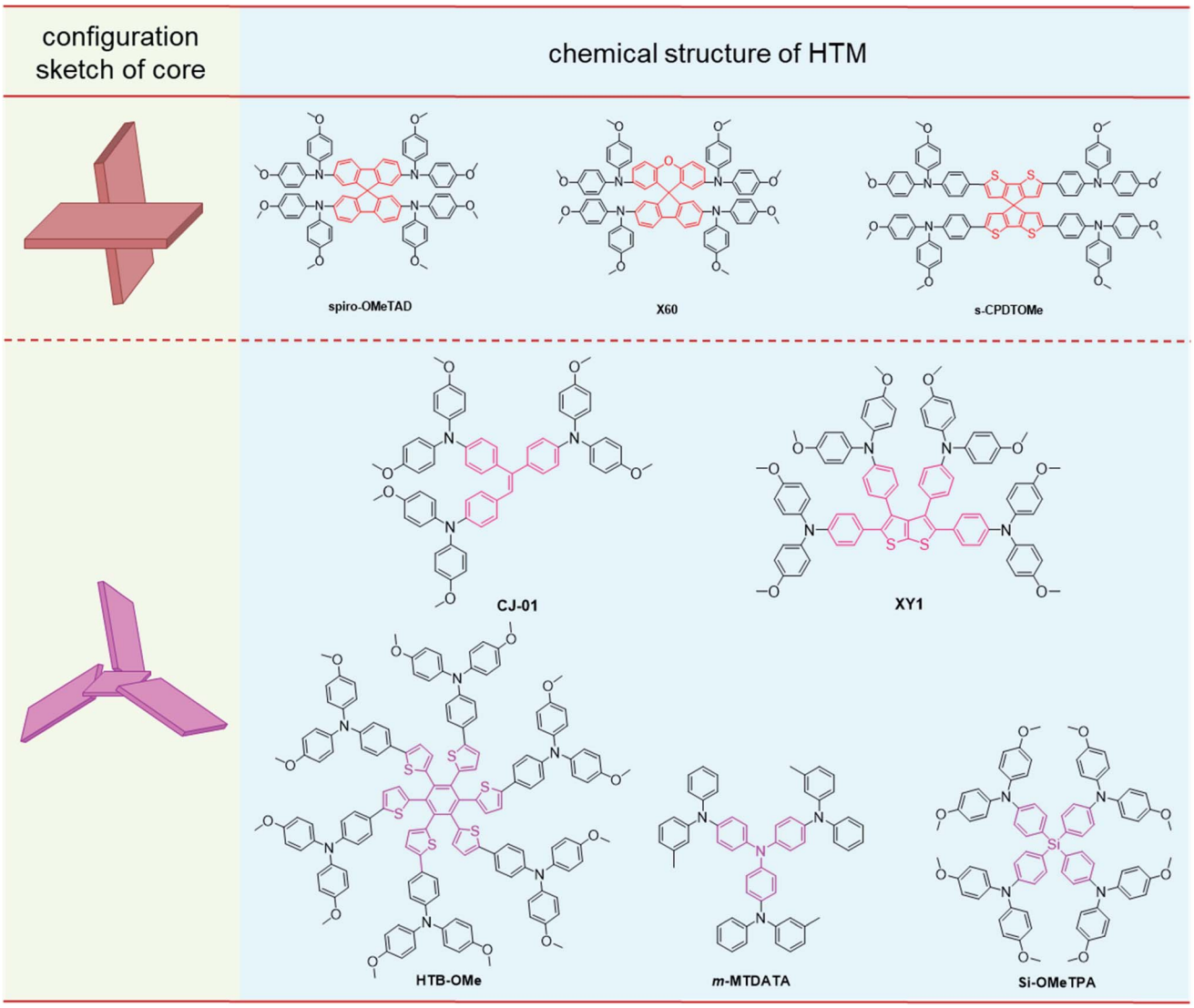

Fig. 4 Configuration sketches of twisted cores and molecular structures of HTMs with twisted cores.

formed in the resultant HTM **HTB-OMe** with triphenylamine derivatives as the peripheral moieties,[61] which showed a high hole mobility of 5.48×10^{-4} cm^2 V^{-1} s^{-1}. The corresponding photovoltaic performance is sensitive to the thickness of HTLs for the varied conductivity and film morphology, and the highest PCE of 17.29% was achieved by the **HTB-OMe** layer with 60 nm thickness in the dopant-free PSC devices, and only 25% loss of the original PCE is obtained after storage for 30 days. Also, triphenylamine (TPA) with the propeller-shaped structure has been applied in HTMs as the core unit.[62–64] ***m*-MTDATA** with the TPA core can form compact films and contribute to the formation of large perovskite crystals in its corresponding inverted PSC devices,[53] which exhibited a hole mobility of 4.4×10^{-5} cm^2 V^{-1} s^{-1} and PCE of 18.12% in the dopant-free PSC device. Once the three-branched structure determined by TPA was changed to the four-branched structure with tetraphenylsilane as the core unit, compound **Si-OMeTPA** could achieve a high hole mobility of 2.96×10^{-4} cm^2 V^{-1} s^{-1} after annealing, and the PCE of its doped device reached 19.06% with an FF of 0.772, while the dopant-free one obtained a PCE of 12.89% and an FF of 0.649.[65]

To optimize molecular packing at the aggregated states, some conjugated planes with fused structures were incorporated into the HTMs as core units. For example, **BDT-POZ**,[66] which consisted of benzo[1,2-*b*:4,5-*b*′]dithiophene (BDT) as the core and *N*-(6-bromohexyl)phenoxazine (POZ) moieties as the peripheral moieties, exhibited compact molecular packing with the distance between the nearest N atoms in two POZ moieties as short as 3.850 Å, contributing to its high hole mobility of 2.1×10^{-4} cm^2 V^{-1} s^{-1}. The dopant-free PSC device based on **BDT-POZ** exhibited a PCE of 19.16% and a high FF of 0.817. With further incorporation of thiophene into the BDT core as the side moiety in **BDT-TPA-*s*Th**,[67] the additional S–π interaction can be formed between the sulfur atoms of the thiophene side chain and the TPA group in the immediate neighbors, resulting in the compact molecular packing of **BDT-TPA-*s*Th** in the film, and the

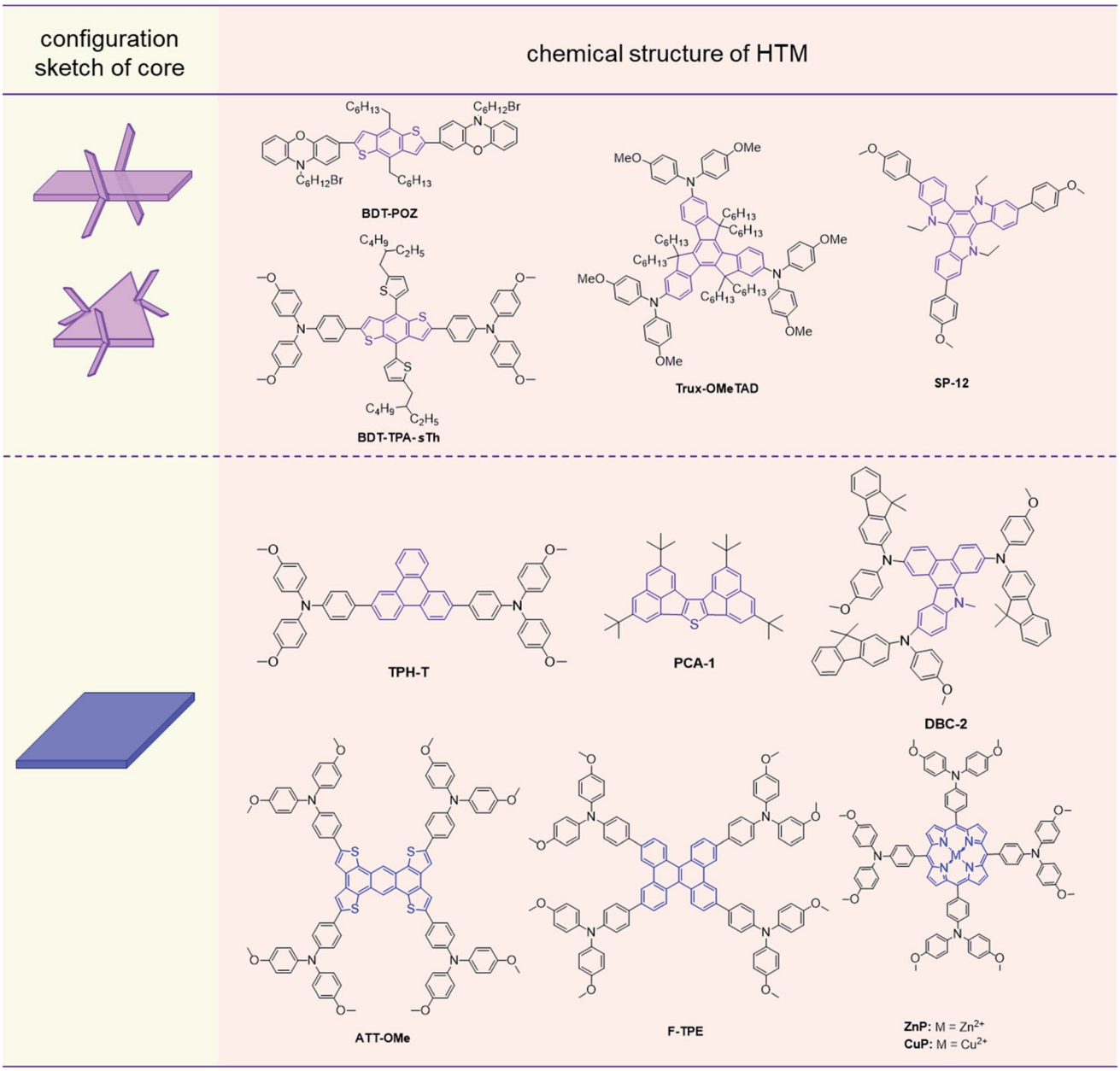

Fig. 5 Configuration sketches of the planar cores and molecular structures of HTMs with planar cores.

hole mobility increased to 5.79×10^{-4} cm^2 V^{-1} s^{-1} after annealing. The PCE of 17.83% was achieved in **BDT-TPA-*s*Th** based dopant-free devices, which could further increase to 20.50% by a solution-processed secondary growth technique. After storage for 500 h, 90% of the initial PCE was still retained from the unencapsulated **BDT-TPA-*s*Th**-based dopant-free devices, and the great stability is mainly due to the compact film with few defects.

Apart from planar cores with linear shapes, some conjugated systems with branched structures and multiple linkage positions were also employed, and several alkyl chains were attached to reduce the possible crystallization in the fabrication process. For instance, truxene with a planar and C_{3h}-symmetric structure was employed in compound **Trux-OMeTAD** as a star-shaped core,[68] which tended to form a face-on molecular packing with a columnar arrangement, resulting in the hole mobility of 3.6×10^{-3} cm^2 V^{-1} s^{-1}. Accordingly, the **Trux-OMeTAD**-based dopant-free PSC exhibited a PCE of 18.6% with an FF of 0.79. Similarly, an alkyl-substituted planar triazatruxene core was applied in **SP-12**,[69] contributing to a high hole mobility of 2.41×10^{-4} cm^2 V^{-1} s^{-1}, and **SP-12**-based doped devices obtained a PCE of 18.8% with a high FF of 0.77.

Also, some fused-ring systems with special shapes have been incorporated, and the varied symmetry has been proved as an efficient approach to adjusting the crystallinity and molecular packing in the aggregated states. For instance, **TPH-T** with a triphenylene core exhibited a hole mobility of 1.83×10^{-4} cm^2 V^{-1} s^{-1} for the optimized π–π interactions, and the corresponding

Table 1 Photovoltaic performances of PSCs applying twisted molecules as HTMs

HTM	Architecture	Perovskite	$\mu_h/10^{-4}$ cm^2 V^{-1} s^{-1}	V_{oc}/V	J_{sc}/mA cm^{-2}	FF	PCE/%	Spiro PCE/%	Ref.
TTE-1	n–i–p (doped)	$(FAPbI_3)_{0.95}(MAPbBr_3)_{0.05}$	0.87	1.03	18.5	0.717	13.68	—	53
TTE-2	n–i–p (doped)	$(FAPbI_3)_{0.95}(MAPbBr_3)_{0.05}$	6.18	1.11	23.4	0.775	20.04	—	53
X60	n–i–p (doped)	$(FAPbI_3)_{0.85}(MAPbBr_3)_{0.15}$	1.9	1.14	24.2	0.71	19.84	—	57
s-CPDTOMe	n–i–p (doped)	$MAPbI_3$	0.30	0.97	19.3	0.72	13.4	15.0	58
CJ-01	n–i–p (doped)	$MAPbI_3$	0.58	1.11	22.3	0.747	18.56	18.69	59
XY1	p–i–n (dopant-free)	$(CsPbI_3)_{0.05}[(FAPbI_3)_{0.83}(MAPbBr_3)_{0.17}]_{0.95}$	3.76	1.11	22.2	0.762	18.78	—	60
HTB-OMe	n–i–p (dopant-free)	$MAPbI_3$	5.48	1.03	22.8	0.737	17.29	—	61
***m*-MTDATA**	p–i–n (dopant-free)	$Cs_{0.05}(FA_{0.85}MA_{0.15})_{0.95}Pb(I_{0.85}Br_{0.15})_3$	0.44	1.04	22.5	0.78	18.12	—	62
Si-OMeTPA	p–i–n (doped)	$MAPbI_3$	0.88	1.07	23.1	0.772	19.06	—	65

Table 2 Photovoltaic performances of PSCs with twisted molecules as HTMs

HTM	Architecture	Perovskite	$\mu_h/10^{-4}$ cm^2 V^{-1} s^{-1}	V_{oc}/V	J_{sc}/mA cm^{-2}	FF	PCE/%	Spiro PCE/%	Ref.
BDT-POZ	p–i–n (dopant-free)	$MAPbI_3$	2.1	1.04	22.6	0.817	19.16	—	66
BDT-TPA-*s*Th	p–i–n (dopant-free)	$MAPbI_3$	5.79	1.15	22.9	0.78	20.50	—	67
Trux-OMeTAD	p–i–n (dopant-free)	$MAPbI_3$	36	1.02	23.2	0.79	18.6	16.3	68
SP-12	n–i–p (doped)	$MAPbI_3$	2.41	1.08	22.8	0.77	18.8	16.9	69
TPH-T	n–i–p (doped)	$(FAPbI_3)_{0.85}(MAPbBr_3)_{0.15}$	1.83	1.11	23.0	0.76	19.4	19.0	70
PCA-1	n–i–p (dopant-free)	$MAPbI_3$	0.83	1.06	22.3	0.767	18.17	—	71
DBC-2	n–i–p (doped)	$MAPbI_{3-x}Cl_x$	9.85	1.11	22.7	0.788	20.02	18.18	73
ATT-OMe	n–i–p (doped)	$(FAPbI_3)_{0.85}(MAPbBr_3)_{0.15}$	—	1.07	21.8	0.781	18.13	17.80	76
F-TPE	n–i–p (doped)	$(FAPbI_3)_{0.85}(MAPbBr_3)_{0.15}$	7.48	1.11	21.4	0.77	18.30	18.16	77
ZnP	n–i–p (dopant-free)	$(FAPbI_3)_{0.85}(MAPbBr_3)_{0.15}$	3.06	1.10	22.7	0.713	17.78	18.59	80
CuP	n–i–p (dopant-free)	$(FAPbI_3)_{0.85}(MAPbBr_3)_{0.15}$	2.89	1.07	21.6	0.663	15.36	18.59	80

PSCs achieved a PCE of 19.4%.[70] Similarly, **PCA-1** with the fused 2,5,9,12-tetra(*tert*-butyl)diacenaphtho[1,2-*b*:1′,2′-*d*]thiophene core demonstrated a PCE of 18.17% in dopant-free devices with a low cost of only $1.02 per g, which is distinctly lower than that of **spiro-OMeTAD** (around $92 per g).[71] Besides, **DBC-2** bearing the dibenzo[*a*,*c*]carbazole (DBC) core with asymmetric structure[72,73] exhibited a hole mobility of 9.85×10^{-4} cm^2 V^{-1} s^{-1} and the PCE of the doped device reached 20.04%.

Once the conjugated planes of cores are further expanded by the incorporation of more aromatics into the fused-ring systems, the strong π–π interactions can be formed in the film, which might result in high crystallinity.[74,75] Thus, some twisted moieties were introduced as peripheral groups to optimize the molecular packing and improve the hole mobility. When four triphenylamine derivatives were attached to the symmetric anthra[1,2-*b*:4,3-*b*′:5,6-*b*″:8,7-*b*‴]tetrathiophene (ATT) core, the resultant **ATT-OMe** as HTM obtained a PCE of 18.13% in the doped devices.[76] A planar fused-tetraphenylethylene by cyclization was applied in **F-TPE** as a core unit,[77] and the roughness of resultant film was 11.2 nm with smooth morphology, and the water-contact angle was 84°, larger than that of the tetraphenylethylene-based analogue (79°), indicating the compact molecular packing in the aggregated states. A high hole mobility of 7.48×10^{-4} cm^2 V^{-1} s^{-1} was achieved by **F-TPE**, and it demonstrated a PCE of 18.30% in doped devices and 13.11% in dopant-free devices. Porphyrin derivatives have also drawn attention for their planar and symmetrical structures.[78,79] Two triphenylamine-substituted porphyrin complexes **CuP** and **ZnP** have been applied as HTMs in dopant-free PSC devices.[80] The intermolecular charge transfer along the π-stacking was enhanced for compact molecular π-stacking, and high hole mobilities of **CuP** (3.06×10^{-4} cm^2 V^{-1} s^{-1}) and **ZnP** (2.89×10^{-4} cm^2 V^{-1} s^{-1}) were achieved; the PCEs of their dopant-free devices were as high as 17.78% and 15.36%, respectively.

2.1.2 Linking types—the linking positions and numbers of peripheral groups. Besides the structures of core units, the molecular configurations of HTMs are also determined by the positions and numbers of peripheral groups (Fig. 6a).

With triarylamine as the peripheral group linked to the different positions of the 9,9-bis(4-diphenylaminophenyl) fluorene (FLTPA) core, **TPA-2,7-FLTPA-TPA** and **TPA-3,6-FLTPA-TPA** (Fig. 6b) exhibited different shapes for the molecular skeletons, with the linear type for **TPA-2,7-FLTPA-TPA**, and the "V" type for **TPA-3,6-FLTPA-TPA.**[89] The twisted skeleton of **TPA-3,6-FLTPA-TPA** has an adverse effect on the intramolecular charge transfer and the possible π–π stacking; accordingly, the **TPA-2,7-FLTPA-TPA**-based device showed a higher FF of 0.78 and PCE of 17.1% than those of **TPA-3,6-FLTPA-TPA** (FF and PCE are 0.67 and 13.9%, respectively). Thus, different linking

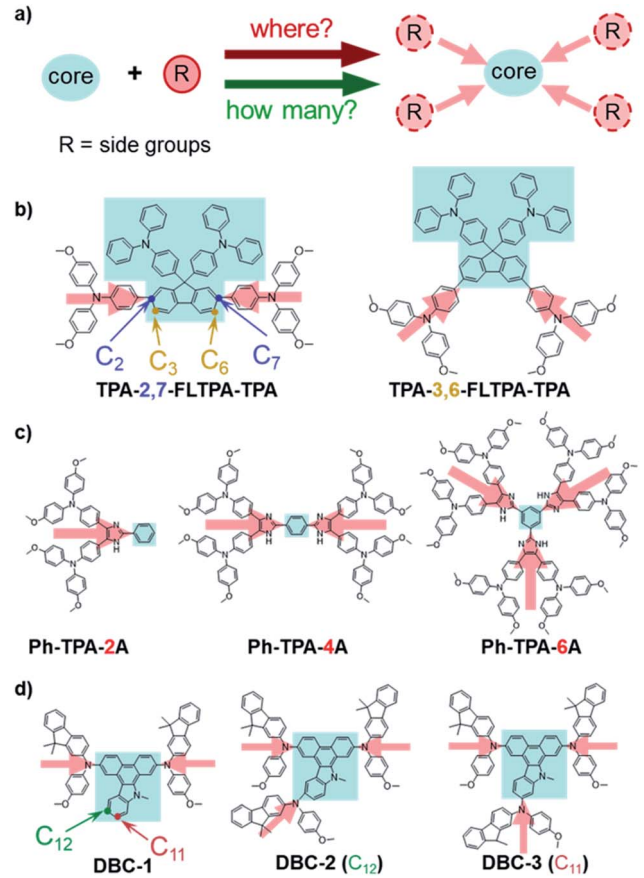

Fig. 6 (a) A sketch of linkage types, including the positions and numbers of peripheral groups. (b) Chemical structures of TPA-2,7-FLTPA-TPA and TPA-3,6-FLTPA-TPA. (c) Chemical structures of Ph-TPA-2A, Ph-TPA-4A and Ph-TPA-6A. (d) Chemical structures of DBC-1, DBC-2 and DBC-3.

positions could decide the molecular shape and planarity, which influenced the molecular packing and further hole-transporting properties.

The numbers of peripheral groups also makes a big difference in the photovoltaic properties of HTMs. **Ph-TPA-2A**, **Ph-TPA-4A** and **Ph-TPA-6A** consist of one, two, or three triarylamines-linked imidazole groups as the peripheral groups and the same benzene core (Fig. 6c).[90] According to the AFM images, the roughness RMS of the **Ph-TPA-4A** film (3.29 nm) is smaller than those of **Ph-TPA-2A** (3.94 nm) and **Ph-TPA-6A** (4.52 nm). The change in the steady-state PL spectra of the perovskite and HTM-coated perovskite exhibited the fastest PL-quenching and hole-extracting in **Ph-TPA-4A** and slowest in **Ph-TPA-2A**. As a result, **Ph-TPA-4A** had the best PCE (18.03%) with the highest J_{sc} of 24.91 mA cm^{-2} and FF of 0.75, as compared to those of **Ph-TPA-6A** (PCE: 13.71%, J_{sc}: 21.80 mA cm^{-2} and FF: 0.62) and **Ph-TPA-2A** (PCE: 12.74%, J_{sc}: 19.79 mA cm^{-2} and FF: 0.62). Both **Ph-TPA-2A** with the smallest number of peripheral groups and **Ph-TPA-6A** with the largest are not good choices for optimizing the photovoltaic performance, while **Ph-TPA-4A** with the medial ones makes a good balance. Therefore, the numbers of peripheral groups may change the symmetry of HTMs and density of the efficient hole-transporting moieties, then impact the hole mobility and extraction.

Our group has reported several HTMs, named **DBC-1**, **DBC-2** and **DBC-3** with the DBC core and different numbers of *N*-(4-methoxyphenyl)-9,9-dimethyl-9*H*-fluorene-2-amine (F(Me)NPh) groups as peripheral moieties (Fig. 6d).[73] By adding one peripheral group to **DBC-1**, the tighter molecular packing of **DBC-2** and **DBC-3** in the film was observed by 2D grazing incidence wide-angle X-ray scattering (2D-GIWAXS) measurements. Compared to **DBC-2**, **DBC-3** with the third F(Me)NPh group substituted at the C_{11} position led to a more planar configuration and tighter π–π stacking for less steric hindrance; however, a higher tendency for crystallization was observed, which resulted in poor film morphology. According to the AFM images, the roughness of **DBC-1**, **DBC-2** and **DBC-3** was 13.91 nm, 11.46 nm and 17.67 nm, respectively. The doped devices of **DBC-2** obtained the highest PCE of 20.02%, higher than 18.81% for **DBC-1** and 16.77% for **DBC-3**, while the PCEs of dopant-free devices of **DBC-1**, **DBC-2** and **DBC-3** were 14.25%, 16.43% and 15.47%, respectively. Therefore, both the linking positions and numbers can influence the molecular planarity and crystallization, which may affect the molecular packing and film-forming properties, then further influence the device performances.

2.2 The main effects of electronic properties on photovoltaic performance

Generally, the electronic properties of HTMs are determined by the building blocks with electron-donating or withdrawing properties. The building blocks of HTMs are mainly electron donors (D) and π-conjugated bridges, which are beneficial for hole extraction and transport in most cases.[91–96] However, the electron-rich properties of HTMs usually result in high HOMO levels, which could decrease the V_{oc} values and stability of devices in principle.[97,98] Thus, the incorporation of electron acceptors (A) was proved to be an efficient approach to deepen the HOMO levels by the intramolecular charge transfer (ICT) in D–A structures.[99–104] Also, the ICT effect can induce charge separation, and the resultant zwitterionic resonance may play a similar role to dopants in HTL to enhance the conductivity.[105] Moreover, the strong dipole–dipole interactions among D–A structures may induce compact molecular packing.[106] Both charge separation and dipole–dipole interactions are favorable to hole transport, and various structures of D–π–D and D–A alternate types of HTMs have been developed (Fig. 7). The chemical structures of selected HTMs with electron acceptors are shown in Fig. 8, with the related photovoltaic performances summarized in Table 3.

The malononitrile moiety with strong electron-withdrawing properties has been applied in many D–A alternating HTMs. Li and coworkers designed an HTM **BTPA-TCNE** of D–A type,[107] in which tricyanovinylene (TCNE) groups were introduced as electron acceptors, and triarylamine groups as electron donors. Tight antiparallel molecular packing was observed through crystal XRD analysis, which could possibly cancel out the negative impact for charge transport from molecular dipole

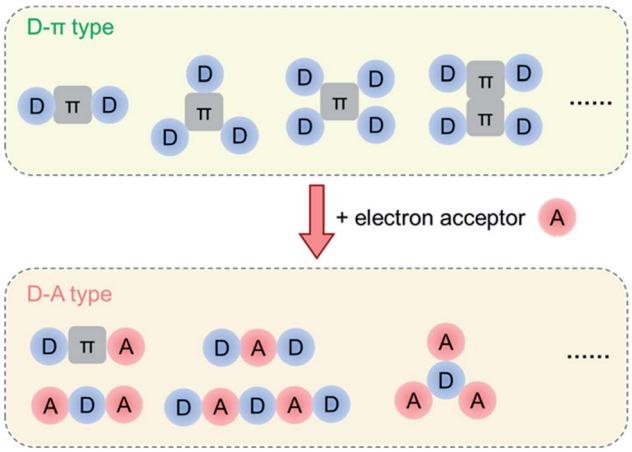

Fig. 7 Schematic representation of D–π and D–A type of HTMs.

moments. Therefore, **BTPA-TCNE** had slightly higher hole mobility (3.14×10^{-5} cm^2 V^{-1} s^{-1}) as compared to that of **BTPA** (1.13×10^{-5} cm^2 V^{-1} s^{-1}) with the removal of the TCNE moiety. The PCEs of **BTPA-TCNE**-based PSCs reached 17.68% (doped device) and 16.94% (dopant-free device), respectively, higher than those of the **BTPA**-based devices (14.07% for doped devices and 4.51% for dopant-free devices). Arora *et al.* designed two D–π–A HTMs **SN5** and **SN6** with dicyanovinylene groups as the electron acceptor and different lengths of π-bridges.[108] Compared to **SN6**, **SN5** with a shorter length of the π-bridge demonstrated the higher PCE (17.7%) in the doped device. This can be attributed to the slightly deeper HOMO of **SN5**, leading to higher V_{oc} (1.043 eV).

The spiro(fluorene-9,9′-xanthene) (SFX) group has been proved to be a potential core for D–π–D HTMs, but low hole mobility leads to the dependence on dopants.[56,109] To improve the hole mobility, Guo and coworkers tried to reduce the electron density of the SFX core by the introduction of fluorine atoms, hoping to enhance the intermolecular dipole–dipole interactions.[110] **2*m*F-X59** with a fluorinated SFX core exhibited a higher hole mobility of 7.14×10^{-5} cm^2 V^{-1} s^{-1} as compared to that of **X59** without fluorine atoms (5.5×10^{-5} cm^2 V^{-1} s^{-1}, previously measured by Bi *et al.*[111]), and the hydrophobicity of **2*m*F-X59** was higher than that of **X59** for the larger water contact angle (100.3° and 95.4° for **2*m*F-X59** and **X59**, respectively). The doped and dopant-free devices of **2*m*F-X59** obtained PCEs of 18.13% and 15.45%, respectively. The high hydrophobicity of **2*m*F-X59** resulted in the great stability of long-term storage, and

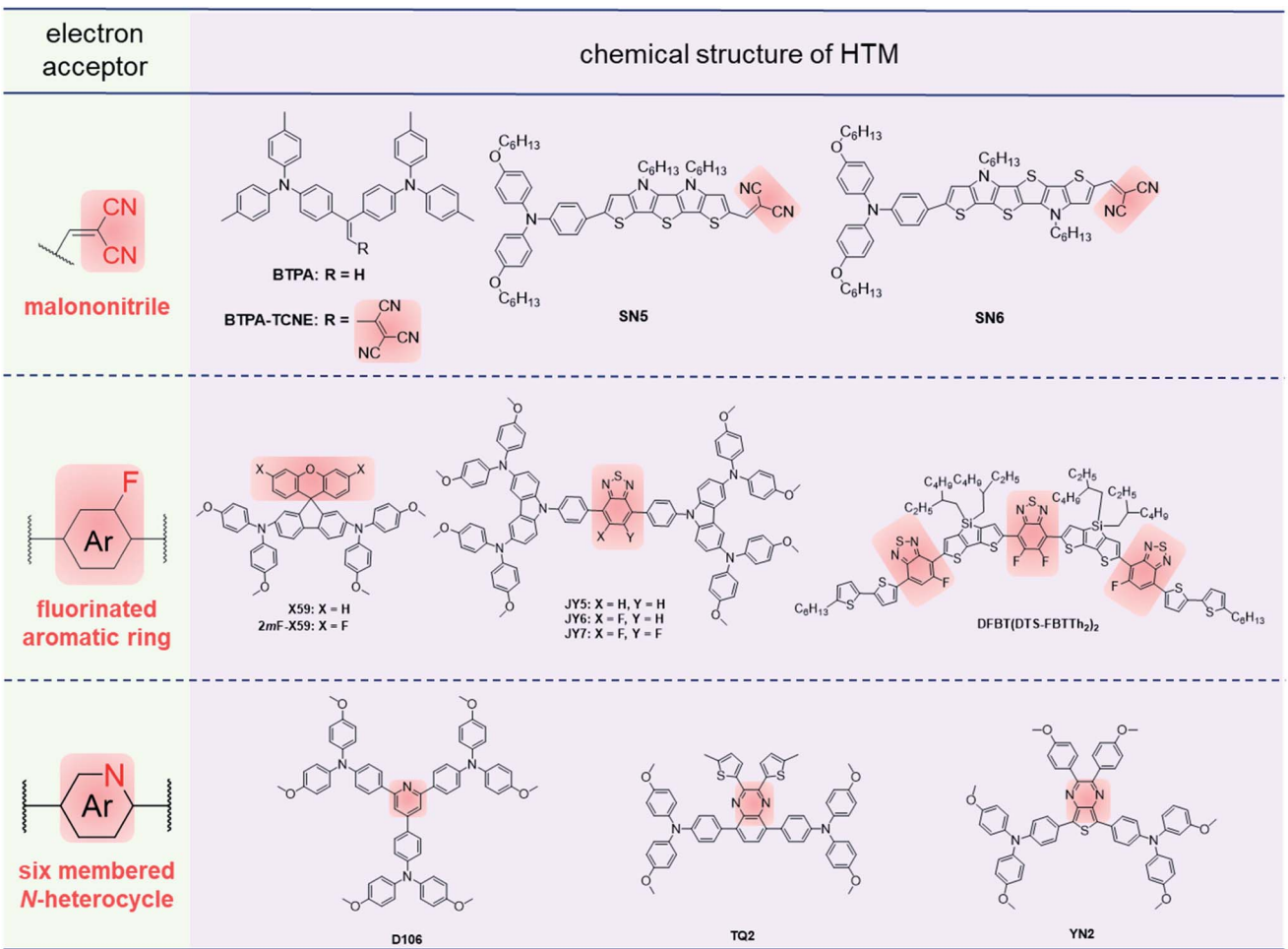

Fig. 8 Sketches of selected electron acceptors and molecular structures of HTMs with D–A alternate type.

Table 3 Photovoltaic performances of PSCs applying some HTMs of the D–A alternate type

HTM	Architecture	Perovskite	$\mu_h/10^{-4}$ cm^2 V^{-1} s^{-1}	V_{oc}/V	J_{sc}/mA cm^{-2}	FF	PCE/%	Spiro PCE/%	Ref.
BTPA-TCNE	n–i–p (doped)	$MAPbI_3$	0.31	1.06	21.1	0.792	17.68	15.70	107
SN5	n–i–p (doped)	$Cs_{0.05}(FA_{0.83}MA_{0.17})_{0.95}Pb(I_{0.83}Br_{0.17})_3$	0.12	1.04	22.5	0.724	17.7	19.8	108
SN6	n–i–p (doped)	$Cs_{0.05}(FA_{0.83}MA_{0.17})_{0.95}Pb(I_{0.83}Br_{0.17})_3$	0.31	1.02	21.7	0.699	16.1	19.8	108
2*m*F-X59	n–i–p (doped)	$MAPbI_3$	0.71	1.01	25.0	0.716	18.13	18.22	110
JY5	n–i–p (doped)	$MAPbI_{3-x}Cl_x$	3.53	1.06	21.1	0.76	16.87	16.24	114
JY6	n–i–p (doped)	$MAPbI_{3-x}Cl_x$	8.84	1.07	21.4	0.81	18.54	16.24	114
JY7	n–i–p (doped)	$MAPbI_{3-x}Cl_x$	4.28	1.05	20.6	0.73	15.71	16.24	114
DFBT(DTS-FBTTh$_2$)$_2$	n–i–p (dopant-free)	$MAPbI_3$	1.78	1.1	20.7	0.760	17.3	17.4	115
D106	p–i–n (dopant-free)	$MAPbI_3$	2.41	1.05	22.3	0.778	18.24	—	119
TQ2	n–i–p (doped)	$MAPbI_3$	2.29	1.12	22.55	0.777	19.62	18.54	120
YN2	n–i–p (dopant-free)	$(FAPbI_3)_{0.85}(MAPbBr_3)_{0.15}$	9.65	1.11	23.15	0.75	19.27	17.80	99

only 5% loss of the initial PCE was observed after 500 h storage without encapsulation.

The fluorinated benzo[*c*][1,2,5]thiadiazole (FBT) group is widely used in D–A alternating HTMs for its suitable electron-withdrawing ability and planar structure.[101,112,113] Zhu *et al.* designed FBT-based HTMs **JY5**, **JY6** and **JY7** with different numbers of fluorine atoms in FBT cores as electron acceptors.[114] **JY6** with one fluorine substituted had the highest PCE of 18.54% in doped devices, while **JY5** and **JY7** exhibited PCEs of 16.87% and 15.71%, respectively. This is mainly related to the varied film morphology, and the high roughness of **JY7** films with pinholes causes poor hole-transporting ability in photovoltaic devices. With multiple D and A moieties incorporated to form the alternate D–A–D–A–D–A–D structures, the resultant **DFBT(DTS-FBTTh$_2$)$_2$** with 4,4-bis(2-ethylhexyl)-4*H*-silolo[3,2-*b*:4,5-*b*′]dithiophene (DTS) as the D unit and FBT with one or two fluorine atoms as acceptors,[115] exhibited strong dipole–dipole interactions at the aggregated states, and a hole mobility of 1.78×10^{-4} cm^2 V^{-1} s^{-1} was obtained in the thin film. Accordingly, the PSC based on **DFBT(DTS-FBTTh$_2$)$_2$** demonstrated a PCE of 17.3% in the dopant-free device.

Besides, six-membered N-heterocycle rings such as pyridine and pyrazine have already been applied as electron-withdrawing units, while the lone pair electrons of N atoms as the feature of Lewis bases might have a passivation effect on Pb^{2+} defects of the perovskite.[116–118] **D106** with 2,4,6-triarylpyridine structure exhibited tight brick-layer packing and intermolecular dipole–dipole interactions in the aggregated states, resulting in a uniform and compact film.[119] Thus, it achieved a high hole mobility of 1.78×10^{-4} cm^2 V^{-1} s^{-1} and PCE of 18.24% in dopant-free devices with a low cost of only $5.62 per g. Also, **TQ2**, with benzopyrazine as the electron acceptor, exhibited a PCE of 19.62% in the doped device,[120] and **YN2** bearing the thienopyrazine moiety demonstrated a PCE of 19.27% in the dopant-free device,[99] indicating the key role of N-heterocycle rings as electron acceptors in the hole transporting properties.

2.3 The synergetic effects of molecular configurations and electronic properties on the photovoltaic performance

Molecular configurations and electronic properties are the key factors in the hole-transporting performances of HTMs. They can impact π–π and dipole–dipole interactions in HTLs, and further influence molecular packing, hole mobility, solubility and film-forming properties. Thus, it is reasonable to take the molecular configurations and electronic properties into consideration when designing efficient HTM molecules.[121–126]

There are several methods for optimizing the effects from molecular configurations and electronic properties since the molecular configuration is mainly tuned by the modification of core units and the electronic properties can be dominated by the introduction of electron acceptor moieties into the core or peripheral moieties, including the incorporation of some electron-withdrawing substituents, and planar electron-deficient conjugated moieties as core units. These two methods are shown in Fig. 9, with their photovoltaic performances summarized in Table 4.

With the cyano-group attached to the conjugated core, **TPA-BFPN-TPA** [127] bearing biphenylfumaronitrile (BFPN) exhibited a hole mobility of 2.9×10^{-4} cm^2 V^{-1} s^{-1} and compact hydrophobic film with a water contact angle of 114°, the PCE of the corresponding dopant-free device reached 18.40%. After exposure under continuous illumination (AM 1.5 G) and humidity of 70% for 100 h, the PCE decreased from 18.4% to 8%, as compared to the PCE of the doped **spiro-OMeTAD** device declining from 16.5% to 5% after only 20 h exposure under similar conditions. **BTF-4** (ref. 128) with the cyano substituted fluoranthene core exhibited a highly ordered herringbone arrangement with edge-to-face packing mode. Compared to the **BTF-2** without cyano groups, **BTF-4** demonstrated a higher hole mobility (1.17×10^{-4} cm^2 V^{-1} s^{-1} for **BTF-4**, 2.13×10^{-5} cm^2 V^{-1} s^{-1} for **BTF-2**), lower series resistance and higher recombination resistance. Moreover, the PCE of **BTF-4** reached 18.03% in the dopant-free n–i–p devices and 17.01% in the p–i–n devices, while those of **BTF-2** were only 10.45% and 11.96%,

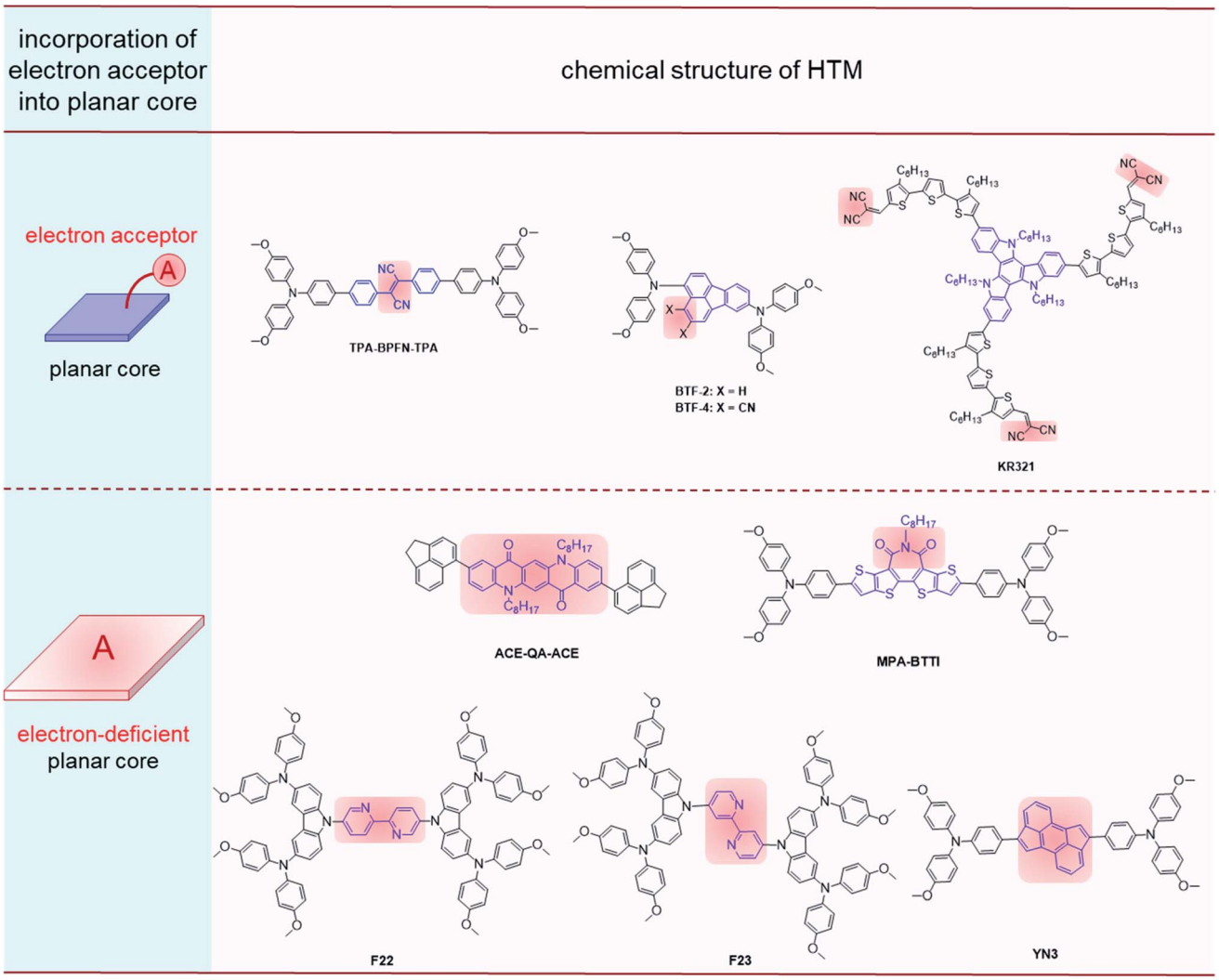

Fig. 9 Molecular structures of HTMs with the synergetic effects of molecular configurations and electronic properties.

Table 4 Photovoltaic performances of PSCs, applying some HTMs of the D–A alternate type with planar cores

HTM	Architecture	Perovskite	$\mu_h/10^{-4}$ cm^2 V^{-1} s^{-1}	V_{oc}/V	J_{sc}/mA cm^{-2}	FF	PCE/%	Spiro PCE/%	Ref.
TPA-BPFN-TPA	n–i–p (dopant-free)	$MAPbI_3$	2.9	1.04	22.70	0.780	18.40	16.60	127
BTF-4	n–i–p (dopant-free)	$(FAPbI_3)_{0.85}(MAPbBr_3)_{0.15}$	1.17	1.06	22.5	0.756	18.03	18.8	128
KR321	n–i–p (dopant-free)	$(FAPbI_3)_{0.85}(MAPbBr_3)_{0.15}$	2.6	1.13	21.70	0.78	19.03	19.01	129
ACE-QA-ACE	n–i–p (dopant-free)	$MAPbI_3$	2.3	1.06	22.41	0.770	18.2	15.2	131
MPA-BTTI	p–i–n (dopant-free)	CsFAMA	2.02	1.12	23.23	0.814	21.17	—	132
F22	n–i–p (dopant-free)	$MAPbI_{3-x}Cl_x$	0.65	1.01	21.11	0.720	15.31	16.94	133
F23	n–i–p (dopant-free)	$MAPbI_{3-x}Cl_x$	1.18	1.07	21.62	0.761	17.60	16.94	133
YN3	n–i–p (dopant-free)	$CsPbI_2Br$	1.98	1.12	22.43	0.75	18.84	18.41	135

respectively. The A–D–A type molecule **KR321** with a planar triazatruxene core and malononitrile groups as the ending groups can form compact molecular π–π stacking with a *d*-spacing of 0.38 nm and face-on molecular orientation, resulting in a high hole mobility of 2.6 × 10^{-4} cm^2 V^{-1} s^{-1} and an excellent PCE of 19.03% with an FF of 0.78 in dopant-free devices.[129]

The carbonyl group has attracted attention for its electron-withdrawing properties and defect passivation effect, which can be combined in various conjugated cores.[130] Once the quinacridone (QA) unit with two ketonic carbonyl groups was incorporated into compound **ACE-QA-ACE**,[131] a high hole mobility of 2.3 × 10^{-4} cm^2 V^{-1} s^{-1} was achieved, and it exhibited a PCE of 18.2% and the FF of 0.770 in dopant-free devices. The core unit in **MPA-BTTI** exhibited a planar

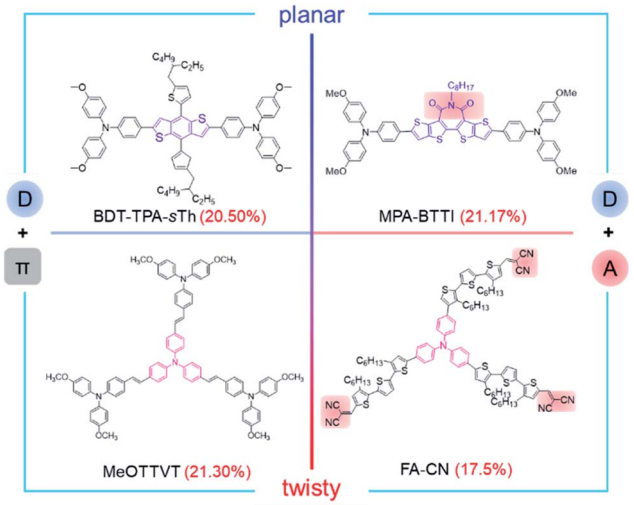

Fig. 10 Excellent photovoltaic performance of PSCs based on dopant-free HTMs with different molecular configurations and electronic properties.[37,67,132,136]

configuration and electron-deficient properties, favoring compact π–π stacking.[132] It also exhibited higher hole mobility (2.02×10^{-4} cm^2 V^{-1} s^{-1}) and conductivity (1.35×10^{-5} S cm^{-1}). **MPA-BTTI** achieved an outstanding PCE of 21.17% in a dopant-free device, with a high FF of 0.814 and V_{oc} of 1.12 V. Moreover, 90% of the initial PCE remained after illumination for 500 h, and 94% after storage at 80 °C for 800 h. This was mainly due to the defect passivation effect, resulting in less charge recombination and better surface contact between the perovskite and HTL.

Bipyridine has a planar structure with electron-withdrawing ability, and there are many sites for substitution, which make it convenient to adjust the energy level, planarity and symmetry.[133,134] Zhu and coworkers applied bipyridine as an electron-withdrawing core in HTM **F22** and **F23** with tunable molecular shapes by the changeable linking positions of peripheral groups;[134] as a consequence, the folded **F23** had a higher hole mobility (1.18×10^{-4} cm^2 V^{-1} s^{-1}) and less film roughness (RMS: 8.92 nm) as compared to the linear **F22** (6.45×10^{-5} cm^2 V^{-1} s^{-1} and 8.92 nm for hole mobility and roughness RMS, respectively), and the dopant-free devices with **F23** as HTL obtained an FF of 0.761 and a PCE of 17.60%, as compared to those of **F22** (FF: 0.720, PCE: 15.31%). The worse photovoltaic performance of **F22** may be related to the symmetrical structure, which can induce high crystallinity in the thin film, leading to poorer film morphology and higher charge recombination. In addition, the cyclopenta[*hi*]aceanthrylene unit, which could also be regarded as a part of the C_{70} fullerene and an electron acceptor, was applied in **YN3** as the core unit to form the D–A–D structure; accordingly, a high hole mobility of 2.25×10^{-4} cm^2 V^{-1} s^{-1} and high PCE of 18.84% were observed in the dopant-free devices.[135]

3. Conclusion

In this review, the relationship between the molecular structures of HTMs and hole-transporting performance in PSC devices is discussed and summarized, and the effects of the molecular configurations and electronic properties of HTMs on the hole-mobility and film morphology are highlighted. Generally, molecular configuration partly determines the molecular packing and intermolecular interactions,[137–142] while electronic property significantly affect intermolecular interactions and charge-transport approaches. Improved photovoltaic performance can be achieved from the molecular level to device fabrication by the rational design of HTMs, together with the optimized perovskite layer and electron-transporting materials.

For doped devices and dopant-free devices, the strategies for the optimization of HTMs are a little different. In general, both the planar configuration and D–A alternating structures of HTMs contribute to high hole mobility, which plays the dominant role in dopant-free devices; alternatively, a twisted configuration is favorable for good solubility and film-forming properties, which are more important to the doped devices.

More and more evidence has proved that dopant-free devices have better stability for storage and long-time work than those of doped devices. Although there is room for improvement, the shortcoming of low stability is increasingly worth the attention for the large-scale applications of PSCs. To solve this problem, more dopant-free HTMs with high efficiency must be developed, and Fig. 10 shows the most efficient dopant-free HTMs with the different kinds of molecular configurations or electron properties reported so far. The film morphology should be further improved on the premise of good solubility, and the technology to analyze the aggregated states of HTMs is also essential and urgent. Normally, the compact film is essential to increase the stability of PSCs by isolating them from the effects of water and oxygen in the air. Also, it can suppress the possible charge recombination to decrease energy loss. A systematic project on adjusting the molecular configuration and electron properties should be carried out to increase the hole mobility, which is the key parameter of the photovoltaic performance.

Recently, many breakthroughs have been reported about the perovskite-silicon tandem solar cells, and over 29% efficiency has been reported so far,[143] which displays great potential for perovskite solar cells. However, there are still some difficulties for commercialization, and material development must be an essential step. As the key element of PSCs, the further requirement of HTLs will be thin films with the perfect compact structures and high hole mobility, which can improve the stability and conversion efficiency together. Accordingly, to achieve these requirements, the electron-deficient cores with planar structures and the optimized molecular configurations by the peripheral moieties with adjustable positions and structures are efficient strategies. Also, the defect passivation effect by HTMs can further enhance the stability and promote carrier transport, equally contributing to the commercialization of PSCs.

Conflicts of interest

There are no conflicts to declare.

Acknowledgements

We are grateful to the National Natural Science Foundation of China (no. 21875174), and Excellent Youth Foundation of Hubei Scientific Committee (2020CFA084), the Fundamental Research Funds for the Central Universities (2042020kf0200) and Wuhan City (2019010701011412) for financial support.

Notes and references

1 Z. Zhou and S. Pang, *J. Mater. Chem. A*, 2020, **8**, 503.
2 J. Ajayan, D. Nirmal, P. Mohankumar, M. Saravanan, M. Jagadesh and L. Arivazhagan, *Superlattices Microstruct.*, 2020, **143**, 106549.
3 P. Roy, N. K. Sinha, S. Tiwari and A. Khare, *Sol. Energy*, 2020, **198**, 665–688.
4 X. Xu, Y. Li and Q. Peng, *Small Struct.*, 2020, **1**, 2000016.
5 X. Xu and X. Wang, *Small Struct.*, 2020, **1**, 2000009.
6 H. Duim, G. H. Ten Brink, S. Adjokatse, R. de Kloe, B. J. Kooi, G. Portable and M. A. Loi, *Small Struct.*, 2020, **1**, 2000074.
7 Q. Yang, M. Wu and X. C. Zeng, *Research*, 2020, **2020**, 1986576.
8 X.-X. Yan, B. Li, H.-S. Lin, F. Jin, C. Niu, K.-Q. Liu, G.-W. Wang and S. Yang, *Research*, 2020, **2020**, 2059190.
9 S. Ma, X. Liu, X. Zhang, R. Ghadari, Y. Ding, M. Cai and S. Dai, *Chem. Commun.*, 2020, **56**, 14471–14474.
10 Q. Jiang, Y. Zhao, X. Zhang, X. Yang, Y. Chen, Z. Chu, Q. Ye, X. Li, Z. Yin and J. You, *Nat. Photonics*, 2019, **13**, 460–466.
11 A. Kojima, K. Teshima, Y. Shirai and T. Miyasaka, *J. Am. Chem. Soc.*, 2009, **131**, 6050–6051.
12 J. Jeong, M. Kim, J. Seo, H. Lu, P. Ahlawat, A. Mishra, Y. Yang, M. A. Hope, F. T. Eickemeyer, M. Kim, Y. J. Yoon, I. W. Choi, B. P. Darwich, S. J. Choi, Y. Jo, J. H. Lee, B. Walker, S. M. Zakeeruddin, L. Emsley, U. Rothlisberger, A. Hagfeldt, D. S. Kim, M. Grätzel and J. Y. Kim, *Nature*, 2021, **592**, 381.
13 F. Liu, Q. Li and Z. Li, *Asian J. Org. Chem.*, 2018, **7**, 2182–2200.
14 J. Urieta-Mora, I. Garcia-Benito, A. Molina-Ontoria and N. Martin, *Chem. Soc. Rev.*, 2018, **47**, 8541.
15 K. Rakstys, C. Igci and M. K. Nazeeruddin, *Chem. Sci.*, 2019, **10**, 6748–6769.
16 Q.-Q. Ge, J.-Y. Shao, J. Ding, L.-Y. Deng, W.-K. Zhou, Y.-X. Chen, J.-Y. Ma, L.-J. Wan, J. Yao, J.-S. Hu and Y.-W. Zhong, *Angew. Chem., Int. Ed.*, 2018, **57**, 10959–10965.
17 T. Braikyla, R. Xia, M. Daskeviciene, T. Malinauskas, A. Gruodis, V. Jankauskas, Z. Fei, C. Momblona, C. R. Carmona, P. J. Dyson, V. Getautis and M. K. Nazeeruddin, *Angew. Chem., Int. Ed.*, 2019, **58**, 11266–11272.
18 Y. Murakami, F. Ishiwari, K. Okamoto, T. Kozawa and A. Saeki, *ACS Appl. Mater. Interfaces*, 2021, **13**, 24824–24832.
19 P. Schulz, E. Edri, S. Kirmayer, G. Hodes, D. Cahen and A. Kahn, *Energy Environ. Sci.*, 2014, **7**, 1377–1381.
20 K. Jiang, J. Wang, F. Wu, Q. Xue, Q. Yao, J. Zhang, Y. Chen, G. Zhang, Z. Zhu, H. Yan, L. Zhu and H.-L. Yip, *Adv. Mater.*, 2020, **32**, 1908011.
21 Z. Yu and L. Sun, *Small Methods*, 2018, **2**, 1700280.
22 W. Yan, S. Ye, Y. Li, W. Sun, H. Rao, Z. Liu, Z. Bian and C. Huang, *Adv. Energy Mater.*, 2016, **6**, 1600474.
23 L. Calió, S. Kazim, M. Grätzel and S. Ahmad, *Angew. Chem., Int. Ed.*, 2016, **55**, 14522–14545.
24 H. Li, N. Tessler and J.-L. Brédas, *Adv. Funct. Mater.*, 2018, **28**, 1803096.
25 H. Zhang, J. Cheng, F. Lin, H. He, J. Mao, K. S. Wong, A. K.-Y. Jen and W. C. H. Choy, *ACS Nano*, 2016, **10**, 1503–1511.
26 N. Arora, M. I. Dar, A. Hinderhofer, N. Pellet, F. Schreiber, S. M. Zakeeruddin and M. Grätzel, *Science*, 2017, **358**, 768–771.
27 J. A. Christians, R. C. M. Fung and P. V. Kamat, *J. Am. Chem. Soc.*, 2014, **136**, 758–764.
28 Z. Hawash, L. K. Ono and Y. Qi, *Adv. Mater. Interfaces*, 2018, **5**, 1700623.
29 E. H. Jung, N. J. Jeon, E. Y. Park, C. S. Moon, T. J. Shin, T.-Y. Yang, J. H. Noh and J. Seo, *Nature*, 2019, **567**, 511–515.
30 N. Y. Nia, F. Matteocci, L. Cina and A. D. Carlo, *ChemSusChem*, 2017, **10**, 3854–3860.
31 J. A. Christians, P. Schulz, J. S. Tinkham, T. H. Schloemer, S. P. Harvey, B. J. T. Villers, A. Sellinger, J. J. Berry and J. M. Luther, *Nat. Energy*, 2018, **3**, 68–74.
32 S. Lee, J. Lee, H. Park, J. Choi, H. W. Baac, S. Park and H. J. Park, *ACS Appl. Mater. Interfaces*, 2020, **12**, 40310–40317.
33 R. Shang, Z. Zhou, H. Nishioka, H. Halim, S. Furukuwa, I. Takei, N. Ninomiya and E. Nakamura, *J. Am. Chem. Soc.*, 2018, **140**, 5018–5022.
34 X. Yang, H. Wang, B. Cai, Z. Yu and L. Sun, *J. Energy Chem.*, 2018, **27**, 650–672.
35 S. Mabrouk, M. Zhang, Z. Wang, M. Liang, B. Bahrami, Y. Wu, J. Wu, Q. Qiao and S. Yang, *J. Mater. Chem. A*, 2018, **6**, 7950–7958.
36 C.-C. Lee, C.-I. Chen, C.-T. Fang, P.-Y. Huang, Y.-T. Wu and C.-C. Chueh, *Adv. Funct. Mater.*, 2019, **29**, 1808625.
37 H. Zhu, Z. Shen, L. Pan, J. Han, F. T. Eickemeyer, Y. Ren, X. Li, S. Wang, H. Liu, X. Dong, S. M. Zakeeruddin, A. Hagfeldt, Y. Liu and M. Grätzel, *ACS Energy Lett.*, 2021, **6**, 208–215.
38 W. Zhou, Z. Wen and P. Gao, *Adv. Energy Mater.*, 2018, **8**, 1702512.
39 H. D. Pham, T. C.-J. Yang, S. M. Jain, G. J. Wilson and P. Sonar, *Adv. Energy Mater.*, 2020, **10**, 1903326.
40 C. Li, R. He, Q. Liang, J. Cao, J. Yin and Y. Tang, *Sci. China: Chem.*, 2020, **63**, 1053–1058.
41 M. Jeong, I. W. Choi, E. M. Go, Y. Cho, M. Kim, B. Lee, S. Jeong, Y. Jo, H. W. Choi, J. Lee, J.-H. Bae, S. K. Kwak, D. S. Kim and C. Yang, *Science*, 2020, **369**, 1615–1620.
42 F. Liu, F. Wu, Z. Tu, Q. Liao, Y. Gong, L. Zhu, Q. Li and Z. Li, *Adv. Funct. Mater.*, 2019, **29**, 1901296.
43 Y. Wang, Q. Liao, J. Chen, W. Huang, X. Zhuang, Y. Tang, B. Li, X. Yao, X. Feng, X. Zhang, M. Su, Z. He, T. J. Marks,

A. Facchetti and X. Guo, *J. Am. Chem. Soc.*, 2020, **142**, 16632–16643.
44 L. Li, Y. Wu, E. Li, C. Shen, H. Zhang, X. Xu, G. Wu, M. Cai and W.-H. Zhu, *Chem. Commun.*, 2019, **55**, 13239–13242.
45 J. Wang, Z. Chai, J. Wang, C. Wang, M. Han, Q. Liao, A. Huang, P. Lin, C. Li, Q. Li and Z. Li, *Angew. Chem., Int. Ed.*, 2019, **58**, 17297–17302.
46 R. Tang and Z. Li, *Chem. Rec.*, 2017, **17**, 71–89.
47 T. Kumari, S. M. Lee, S.-H. Kang, S. Chen and C. Yang, *Energy Environ. Sci.*, 2017, **10**, 258–265.
48 Q. Li and Z. Li, *Acc. Chem. Res.*, 2020, **53**, 962–973.
49 J. Seo, J. H. Noh and S. I. Seok, *Acc. Chem. Res.*, 2016, **49**, 562–572.
50 J. Wang, H. Zhang, B. Wu, Z. Wang, Z. Sun, S. Xue, Y. Wu, A. Hagfeldt and M. Liang, *Angew. Chem., Int. Ed.*, 2019, **58**, 15721–15725.
51 G. Kim, H. Min, K. S. Lee, D. Y. Lee, S. M. Yoon and S. I. Seok, *Science*, 2020, **370**, 108–112.
52 D. Shi, X. Qin, Y. Li, Y. He, C. Zhong, J. Pan, H. Dong, W. Xu, T. Li, W. Hu, J.-L. Brédas and O. M. Bakr, *Sci. Adv.*, 2016, **2**, e1501491.
53 C. Shen, Y. Wu, H. Zhang, E. Li, W. Zhang, X. Xu, W. Wu, H. Tian and W.-H. Zhu, *Angew. Chem., Int. Ed.*, 2019, **58**, 3784–3789.
54 M. M. Montoya, P. Gómez, D. Curiel, I. Silva, J. Wang and R. A. J. Janssen, *Chem.–Eur. J.*, 2020, **26**, 10276–10282.
55 B. Cai, X. Yang, X. Jiang, Z. Yu, A. Hagfeldt and L. Sun, *J. Mater. Chem. A*, 2019, **7**, 14835–14841.
56 X. Wang, J. Zhang, S. Yu, W. Yu, P. Fu, X. Liu, D. Tu, X. Guo and C. Li, *Angew. Chem., Int. Ed.*, 2018, **57**, 12529–12533.
57 B. Xu, D. Bi, Y. Hua, P. Liu, M. Cheng, M. Grätzel, L. Kloo, A. Hagfeldt and L. Sun, *Energy Environ. Sci.*, 2016, **9**, 873–877.
58 M. Franckevičius, A. Mishra, F. Kreuzer, J. Luo, S. M. Zakeeruddin and M. Grätzel, *Mater. Horiz.*, 2015, **2**, 613–618.
59 J. Chen, J. Xia, H.-J. Yu, J.-X. Zhong, X.-K. Wu, Y.-S. Qin, C. Jia, Z. She, D.-B. Kuang and G. Shao, *Chem. Mater.*, 2019, **31**, 5431–5441.
60 X. Yang, J. Xi, Y. Sun, Y. Zhang, G. Zhou and W.-Y. Wong, *Nano Energy*, 2019, **64**, 103946.
61 B.-B. Cui, Y. Han, N. Yang, S. Yang, L. Zhang, Y. Wang, Y. Jia, L. Zhao, Y.-W. Zhong and Q. Chen, *ACS Appl. Mater. Interfaces*, 2018, **10**, 41592–41598.
62 R. Chen, T. Bu, J. Li, W. Li, P. Zhou, X. Liu, Z. Ku, J. Zhong, Y. Peng, F. Huang, Y.-B. Cheng and Z. Fu, *ChemSusChem*, 2018, **11**, 1467–1473.
63 X. Zhao, F. Zhang, C. Yi, D. Bi, X. Bi, P. Wei, J. Luo, X. Liu, S. Wang, X. Li, S. M. Zakeeruddin and M. Grätzel, *J. Mater. Chem. A*, 2016, **4**, 16330–16334.
64 F. Zhang, X. Liu, C. Yi, D. Bi, J. Luo, S. Wang, X. Li, Y. Xiao, S. M. Zakeeruddin and M. Grätzel, *ChemSusChem*, 2016, **9**, 2578–2585.
65 R. Xue, M. Zhang, G. Xu, J. Zhang, W. Chen, H. Chen, M. Yang, C. Cui, Y. Li and Y. Li, *J. Mater. Chem. A*, 2018, **6**, 404–413.
66 Y. Chen, X. Xu, N. Cai, S. Qian, R. Luo, Y. Huo and S.-W. Tsang, *Adv. Energy Mater.*, 2019, **9**, 1901268.
67 R. Xue, M. Zhang, D. Luo, W. Chen, R. Zhu, Y. Yang, Y. Li and Y. Li, *Sci. China: Chem.*, 2020, **63**, 987–996.
68 C. Huang, W. Fu, C.-Z. Li, Z. Zhang, W. Qiu, M. Shi, P. Heremans, A. K.-Y. Jen and H. Chen, *J. Am. Chem. Soc.*, 2016, **138**, 2528–2531.
69 P.-Y. Su, L.-B. Huang, J.-M. Liu, Y.-F. Chen, L.-M. Xiao, D.-B. Kuang, M. Mayor and C.-Y. Su, *J. Mater. Chem. A*, 2017, **5**, 1913–1918.
70 W. Chen, H. Zhang, H. Zheng, H. Li, F. Guo, G. Ni, M. Ma, C. Shi, R. Ghadari and L. Hu, *Chem. Commun.*, 2020, **56**, 1879–1882.
71 Y. Li, K. R. Scheel, R. G. Clevenger, W. Shou, H. Pan, K. V. Kilway and Z. Peng, *Adv. Energy Mater.*, 2018, **8**, 1801248.
72 F. Liu, Q. Liao, J. Wang, Y. Gong, Q. Dang, W. Ling, M. Han, Q. Li and Z. Li, *Sci. China: Chem.*, 2020, **63**, 1435–1442.
73 F. Liu, F. Wu, W. Ling, Z. Tu, J. Zhang, Z. Wei, L. Zhu, Q. Li and Z. Li, *ACS Energy Lett.*, 2019, **4**, 2514–2521.
74 H. D. Pham, T. T. Do, J. Kim, C. Charbonneau, S. Manzhos, K. Feron, W. C. Tsoi, J. R. Durrant, S. M. Jain and P. Sonar, *Adv. Energy Mater.*, 2018, **8**, 1703007.
75 J. U. Mora, I. Zimmermann, J. Aragó, A. M. Ontoria, E. Ortí, N. Martín and M. K. Nazeeruddin, *Chem. Mater.*, 2019, **31**, 6435–6442.
76 I. Zimmermann, J. U. Mora, P. Gratia, J. Aragó, G. Grancini, A. M. Ontoria, E. Ortí, N. Martín and M. K. Nazeeruddin, *Adv. Energy Mater.*, 2017, **7**, 1601674.
77 X. Zhang, Z. Zhou, S. Ma, G. Wu, X. Liu, M. Mateen, R. Ghadari, Y. Wu, Y. Ding, M. Cai and S. Dai, *Chem. Commun.*, 2020, **56**, 3159–3162.
78 Y.-H. Chiang, H.-H. Chou, W.-T. Cheng, Y.-R. Li, C.-Y. Yeh and P. Chen, *ACS Energy Lett.*, 2018, **3**, 1620–1626.
79 M. Urbani, G. Torre, M. K. Nazeeruddin and T. Torres, *Chem. Soc. Rev.*, 2019, **48**, 2738–2766.
80 S. Chen, P. Liu, Y. Hua, Y. Li, L. Kloo, X. Wang, B. Ong, W.-K. Wong and X. Zhu, *ACS Appl. Mater. Interfaces*, 2017, **9**, 13231–13239.
81 Y. Wang, Z. Zhu, C.-C. Chueh, A. K.-J. Jen and Y. Chi, *Adv. Energy Mater.*, 2017, **7**, 1700823.
82 J. Zhang, B. Xu, L. Yang, C. Ruan, L. Wang, P. Liu, W. Zhang, N. Vlachopoulos, L. Kloo, G. Boschloo, L. Sun, A. Hagfeldt and E. M. J. Johansson, *Adv. Energy Mater.*, 2018, **8**, 1701209.
83 M.-H. Li, C.-W. Hsu, P.-S. Shen, H.-M. Cheng, Y. Chi, P. Chen and T.-F. Guo, *Chem. Commun.*, 2015, **51**, 15518–15521.
84 R. Grisorio, R. Iacobellis, A. Listorti, L. D. Marco, M. P. Cipolla, M. Manca, A. Rizzo, A. Abate, G. Gigli and G. P. Suranna, *ACS Appl. Mater. Interfaces*, 2017, **9**, 24778–24787.
85 I. G. Benito, I. Zimmermann, J. U. Mora, J. Aragó, J. Calbo, J. Perles, A. Serrano, A. M. Ontoria, E. Ortí, N. Martín and M. K. Nazeeruddin, *Adv. Funct. Mater.*, 2018, **28**, 1801734.
86 I. Petrikyte, I. Zimmermann, K. Rakstys, M. Daskeviciene, T. Malinauskas, V. Jankauskas, V. Getautis and M. K. Nazeeruddin, *Nanoscale*, 2016, **8**, 8530–8535.

87 H.-A. Lin, N. Mitoma, L. Meng, Y. Segawa, A. Wakamiya and K. Itami, *Mater. Chem. Front.*, 2018, **2**, 275–280.
88 X.-C. Li, Y.-G. Tu, C. Meng, W. Song, T. Cheng, Y.-T. Gong, J. Min, R. Zhu, W.-Y. Lai and W. Huang, *ACS Appl. Mater. Interfaces*, 2019, **11**, 45717–45725.
89 H. D. Pham, L. G. Escrig, K. Feron, S. Manzhos, S. Albrecht, H. J. Bolink and P. Sonar, *J. Mater. Chem. A*, 2019, **7**, 12507–12517.
90 J.-Y. Feng, K.-W. Lai, Y.-S. Shiue, A. Singh, C. H. P. Kumar, C.-T. Li, W.-T. Wu, J. T. Lin, C.-W. Chu, C.-C. Chang and C. Su, *J. Mater. Chem. A*, 2019, **7**, 14209–14221.
91 A. M. Ontoria, I. Zimmermann, I. G. Benito, P. Gratia, C. R. Carmona, S. Aghazada, M. Graetzel, M. K. Nazeeruddin and N. Martín, *Angew. Chem.*, 2016, **128**, 6378–6382.
92 Y.-L. Xu, W.-L. Ding and Z.-Z. Sun, *Nanoscale*, 2018, **10**, 20329–20338.
93 W. Hu, Z. Zhang, J. Cui, W. Shen, M. Li and R. He, *Nanoscale*, 2017, **9**, 12916–12924.
94 F. Zhang, S. Wang, H. Zhu, X. Liu, H. Liu, X. Li, Y. Xiao, S. M. Zakeeruddin and M. Grätzel, *ACS Energy Lett.*, 2018, **3**, 1145–1152.
95 X. Jia, Y. Zhang, J. Zhang, Q. Sun, H. Guo, Y. Wang, S. Zhang, N. Yuan and J. Ding, *Sci. China: Chem.*, 2020, **63**, 827–832.
96 F. Zhang, Z. Wang, H. Zhu, N. Pellet, J. Luo, C. Yi, X. Liu, H. Liu, S. Wang, X. Li, Y. Xiao, S. M. Zakeeruddin, D. Bi and M. Grätzel, *Nano Energy*, 2017, **41**, 469–475.
97 S. Paek, I. Zimmermann, P. Gao, P. Gratia, K. Rakstys, G. Grancini, M. K. Nazeeruddin, M. A. Rub, S. A. Kosa, K. A. Alamry and A. M. Asiri, *Chem. Sci.*, 2016, **7**, 6068–6075.
98 Y. Wu and W. Zhu, *Chem. Soc. Rev.*, 2013, **42**, 2039.
99 P. Xu, P. Liu, Y. Li, B. Xu, L. Kloo, L. Sun and Y. Hua, *ACS Appl. Mater. Interfaces*, 2018, **10**, 19697–19703.
100 X. Sun, F. Wu, C. Zhong, L. Zhu and Z. Li, *Chem. Sci.*, 2019, **10**, 6899–6907.
101 G.-W. Kim, J. Kim, G.-Y. Lee, G. Kang, J. Lee and T. Park, *Adv. Energy Mater.*, 2015, **5**, 1500471.
102 Y.-C. Chen, S.-K. Huang, S.-S. Li, Y.-Y. Tsai, C.-P. Chen, C.-W. Chen and Y. J. Chang, *ChemSusChem*, 2018, **11**, 3225–3233.
103 J.-H. Lee, J. Kim, G. Kim, D. Shin, S. Y. Jeong, J. Lee, S. Hong, J. W. Choi, C.-L. Lee, H. Kim, Y. YI and K. Lee, *Energy Environ. Sci.*, 2018, **11**, 1742–1751.
104 K. Lim, M.-S. Kang, Y. Myung, J.-H. Seo, P. Banerjee, T. J. Marks and J. Ko, *J. Mater. Chem. A*, 2016, **4**, 1186–1190.
105 Q. Xiao, F. Wu, M. Han, Z. Li, L. Zhu and Z. Li, *J. Mater. Chem. A*, 2018, **6**, 13644–13651.
106 B. H. Robinson and L. R. Dalton, *J. Phys. Chem. A*, 2000, **104**, 4785–4795.
107 Z. Li, Z. Zhu, C.-C. Chueh, S. B. Jo, J. Luo, S.-H. Jang and A. K.-Y. Jen, *J. Am. Chem. Soc.*, 2016, **138**, 11833–11839.
108 N. Arora, C. Wetzel, M. I. Dar, A. Mishra, P. Yadav, C. Steck, S. M. Zakeeruddin, P. Bäuerle and M. Grätzel, *ACS Appl. Mater. Interfaces*, 2017, **9**, 44423–44428.
109 K. Liu, Y. Yao, J. Wang, L. Zhu, M. Sun, B. Ren, L. Xie, Y. Luo, Q. Meng and X. Zhan, *Mater. Chem. Front.*, 2017, **1**, 100–110.
110 K. Guo, M. Wu, S. Yang, Z. Wang, J. Li, X. Liang, F. Zhang, Z. Liu and Z. Wang, *Sol. RRL*, 2019, **3**, 1800352.
111 D. Bi, B. Xu, P. Gao, L. Sun, M. Grätzel and A. Hagfeldt, *Nano Energy*, 2016, **23**, 138–144.
112 J. H. Heo, S. H. Im, J. H. Noh, T. N. Mandal, C.-S. Lim, J. A. Chang, Y. H. Lee, H.-J. Kim, A. Sarkar, M. K. Nazeeruddin, M. Grätzel and S. Il Seok, *Nat. Photonics*, 2013, **7**, 486–491.
113 Y. Liu, Z. Hong, Q. Chen, H. Chen, W.-H. Chang, Y. Yang, T.-B. Song and Y. Yang, *Adv. Mater.*, 2016, **28**, 440–446.
114 F. Wu, Y. Ji, C. Zhong, Y. Liu, L. Tan and L. Zhu, *Chem. Commun.*, 2017, **53**, 8719–8722.
115 J. H. Heo, S. Park, S. H. Im and H. J. Son, *ACS Appl. Mater. Interfaces*, 2017, **9**, 39511–39518.
116 S. S. Reddy, V. M. Arivunithi, V. G. Sree, H. Kwon, J. Park, Y.-C. Kang, H. Zhu, Y.-Y. Noh and S.-H. Jin, *Nano Energy*, 2019, **58**, 284–292.
117 Y. Ji, B. He, H. Lu, J. Xu, R. Wang, Y. Jin, C. Zhong, Y. Shan, F. Wu and L. Zhu, *ChemSusChem*, 2019, **12**, 1374–1380.
118 B. Xu, Z. Zhu, J. Zhang, H. Liu, C.-C. Chueh, X. Li and A. K.-Y. Jen, *Adv. Energy Mater.*, 2017, **7**, 1700683.
119 L. Duan, Y. Chen, J. Jia, X. Zong, Z. Sun, Q. Wu and S. Xue, *ACS Appl. Energy Mater.*, 2020, **3**, 1672–1683.
120 H. Zhang, Y. Wu, W. Zhang, E. Li, C. Shen, H. Jiang, H. Tian and W.-H. Zhu, *Chem. Sci.*, 2018, **9**, 5919–5928.
121 M. L. Petrus, K. Schutt, M. T. Sirtl, E. M. Hutter, A. C. Closs, J. M. Ball, J. C. Bijleveld, A. Petrozza, T. Bein, T. J. Dingemans, T. J. Savenije, H. Snaith and P. Docampo, *Adv. Energy Mater.*, 2018, **8**, 1801605.
122 M. Cheng, B. Xu, C. Chen, X. Yang, F. Zhang, Q. Tan, Y. Hua, L. Kloo and L. Sun, *Adv. Energy Mater.*, 2015, **5**, 1401720.
123 P. Qin, H. Kast, M. K. Nazeeruddin, S. M. Zakeeruddin, A. Mishra, P. Bäuerle and M. Grätzel, *Energy Environ. Sci.*, 2014, **7**, 2981–2985.
124 X. Liu, S. Ma, Y. Ding, J. Gao, X. Liu, J. Yao and S. Dai, *Sol. RRL*, 2019, **3**, 1800337.
125 G.-W. Kim, J. Lee, G. Kang, T. Kim and T. Park, *Adv. Energy Mater.*, 2018, **8**, 1701935.
126 H.-C. Liao, T. L. D. Tam, P. Guo, Y. Wu, E. F. Manley, W. Huang, N. Zhou, C. M. M. Soe, B. Wang, M. R. Wasielewski, L. X. Chen, M. G. Kanatzidis, A. Facchetti, R. P. H. Chang and T. J. Marks, *Adv. Energy Mater.*, 2016, **6**, 1600502.
127 H. D. Pham, S. M. Jain, M. Li, Z.-K. Wang, S. Manzhos, K. Feron, S. Pitchaimuthu, Z. Liu, N. Motta, J. R. Durrant and P. Sonar, *Adv. Electron. Mater.*, 2020, **6**, 1900884.
128 X. Sun, Q. Xue, Z. Zhu, Q. Xiao, K. Jiang, H.-L. Yip, H. Yan and Z. Li, *Chem. Sci.*, 2018, **9**, 2698–2704.
129 K. Rakstys, S. Paek, P. Gao, P. Gratia, T. Marszalek, G. Grancini, K. T. Cho, K. Genevicius, V. Jankauskas, W. Pisula and M. K. Nazeeruddin, *J. Mater. Chem. A*, 2017, **5**, 7811–7815.

130 Y. Lin, L. Shen, J. Dai, Y. Deng, Y. Wu, Y. Bai, X. Zheng, J. Wang, Y. Fang, H. Wei, W. Ma, X. C. Zeng, X. Zhan and J. Huang, *Adv. Mater.*, 2017, **29**, 1604545.
131 H. D. Pham, S. M. Jain, M. Li, S. Manzhos, K. Feron, S. Pitchaimuthu, Z. Liu, N. Motta, H. Wang, J. R. Durrant and P. Sonar, *J. Mater. Chem. A*, 2019, **7**, 5315–5323.
132 Y. Wang, W. Chen, L. Wang, B. Tu, T. Chen, B. Liu, K. Yang, C. W. Koh, X. Zhang, H. Sun, G. Chen, X. Feng, H. Y. Woo, A. B. Djurišić, Z. He and X. Guo, *Adv. Mater.*, 2019, **31**, 1902781.
133 H. Lu, B. He, Y. Ji, Y. Shan, C. Zhong, J. Xu, J. LiuYang, F. Wu and L. Zhu, *Chem. Eng. J.*, 2020, **385**, 123976.
134 F. Wu, Y. Shan, J. Qiao, C. Zhong, R. Wang, Q. Song and L. Zhu, *ChemSusChem*, 2017, **10**, 3833–3838.
135 D. Zhang, P. Xu, T. Wu, Y. Ou, X. Yang, A. Sun, B. Cui, H. Sun and Y. Hua, *J. Mater. Chem. A*, 2019, **7**, 5221–5226.
136 S. Paek, P. Qin, Y. Lee, K. T. Cho, P. Gao, G. Grancini, E. Oveisi, P. Gratia, K. Rakstys, S. A. Al-Muhtaseb, C. Ludwig, J. Ko and M. K. Nazeeruddin, *Adv. Mater.*, 2017, **29**, 1606555.
137 Q. Li and Z. Li, *Adv. Sci.*, 2017, **4**, 1600484.
138 Q. Li, Y. Tang, W. Hu and Z. Li, *Small*, 2018, **14**, 1801560.
139 Y. Fan, Q. Li and Z. Li, *Mater. Chem. Front.*, 2021, **5**, 1525–1540.
140 Q. Li and Z. Li, *Sci. China Mater.*, 2020, **63**, 177–184.
141 M. Jin, Z. Zhu, Q. Liao, Q. Li and Z. Li, *Chin. J. Polym. Sci.*, 2020, **38**, 118–125.
142 F. Liu, S. Bi, X. Wang, X. Leng, M. Han, B. Xue, Q. Li, H. Zhou and Z. Li, *Sci. China: Chem.*, 2019, **62**, 739–745.
143 A. Al-Ashouri, E. Köhnen, B. Li, A. Magomedov, H. Hempel, P. Caprioglio, J. A. Márquez, A. B. M. Vilches, E. Kasparavicius, J. A. Smith, N. Phung, D. Menzel, M. Grischek, L. Kegelmann, D. Skroblin, C. Gollwitzer, T. Malinauskas, M. Jošt, G. Matič, B. Rech, R. Schlatmann, M. Topič, L. Korte, A. Abate, B. Stannowski, D. Neher, M. Stolterfoht, T. Unold, V. Getauti and S. Albrecht, *Science*, 2020, **370**, 1300–1309.